Quantitative photon tunneling and shear-force microscopy of planar waveguide splitters and mixers

M. L. M. Balistreri,[a] J. P. Korterik, G. J. Veldhuis,[a] L. Kuipers, and N. F. van Hulst[b]
Applied Optics Group and Lightwave Device Group, MESA$^+$ Research Institute and Department of Applied Physics, University of Twente, P.O. Box 217, 7500 AE Enschede, The Netherlands

(Received 19 June 2000; accepted for publication 18 December 2000)

A combined photon scanning tunneling and shear-force microscope has been developed to investigate the optical field distribution in a planar waveguide splitter and a multibranch mode mixer. The optical intensity distribution just above the surface of a planar waveguide is mapped with subwavelength resolution by a tapered optical fiber that probes the evanescent field. Simultaneously, the topography of the waveguide is recorded with subnanometer accuracy using a constant-distance feedback system based on shear-force detection with a tuning fork sensor. The experimental field patterns are quantitatively compared with field patterns simulated with the two-dimensional finite difference beam propagation method and a−mode solver. Good quantitative agreement between experiment and simulation is obtained. Moreover, the experiment reveals several details in the field distribution that results from incoupling conditions, mask imperfections, waveguide edges, and surface roughness. The surface effects in the optical field distribution are introduced by the use of the constant-distance feedback system. © *2001 American Institute of Physics.*
[DOI: 10.1063/1.1347952]

I. INTRODUCTION

Integrated optical waveguide devices, like straight channels, splitters, and mixers are central to numerous applications in optical telecommunication and information processing systems. An accurate knowledge of the field distribution of the light in the waveguides, the refractive index, and the dimensions of such waveguides is essential for designing and optimizing integrated optical waveguide devices. Most characterization methods are based on the ''black-box'' type methods: the relation between the known incoming light and the measured outcoming light is compared and confronted with a theoretical model.[1] What actually occurs inside the structure remains hidden. Determination of the field distribution of the light is impossible using these methods. Some of the approaches are even destructive and measure the dimensions of the waveguides only indirectly and not locally. Conventional optical microscopy is often used to image indirectly the field distribution of the light in the waveguides by detecting the light scattered at the surface of the waveguide.[2,3] The resolution of this latter method is diffraction limited to at best about half of the wavelength of the detected light. Moreover, light scattering is a loss factor in waveguides. High-quality/low-loss waveguides are difficult to image while relying on scattering. With this method, it is possible to measure the dimensions of the waveguides locally, but not accurately and not directly. The refractive index can be measured with some of the characterization methods directly, but not locally. Obviously, it is preferable to measure the field distribution of the light, the refractive index and the dimensions of the waveguides directly and simultaneously. Moreover, it is desirable to measure the field distribution of the light in high-quality/low-loss waveguides nondestructively and *in situ* with a resolution beyond the diffraction limit. Finally, the method should be sensitive enough to measure subwavelength optical features in the waveguide, but also capable of imaging long waveguides with lengths ranging from a couple of millimeters to several centimeters.

With a near-field scanning optical microscope (NSOM), it is possible to produce optical images of surfaces with subwavelength resolution.[4] In these microscopes, a coated fiber probe with an aperture, much smaller than the optical wavelength, acting as a point source or detector, is scanned over a surface. The optical resolution of the coated fiber probe is determined by the size of the aperture.[4] A reflection type NSOM[5] is well suited for the observation of refractive index changes in waveguides, but unfortunately not for the detecting of the field distribution of the light in the waveguides. The photon scanning tunneling microscope (PSTM) is an alternative type of the NSOM that uses the fiber probe as detector to measure directly the evanescent field of a sample at the air–sample interface.[6–10] The fiber probe is raster scanned above the interface while the distance between the interface and the fiber probe is kept constant. The evanescent wave is locally converted into a propagating wave, due to photon tunneling and guided through the fiber, as is schematically shown in Fig. 1. Several groups,[5,11–20] including our group,[11–13] have shown that the PSTM can be used to characterize integrated optical waveguides. For example, Choo *et al.*[21] have imaged the optical power transfer in a directional coupler over a length of 2 mm. The mode-cutoff wavelengths and the local refractive index changes of channel waveguides have been determined by Bourillot *et al.*[15] Our group has demonstrated the use of microfabricated can-

[a]Present address: Philips, 5656 AA Eindhoven, The Netherlands.
[b]Electronic mail: nf.vanhulst@tn.utwente.nl

 © 2001 American Institute of Physics

Downloaded 01 Sep 2003 to 130.89.25.109. Redistribution subject to AIP license or copyright, see http://ojps.aip.org/japo/japcr.jsp

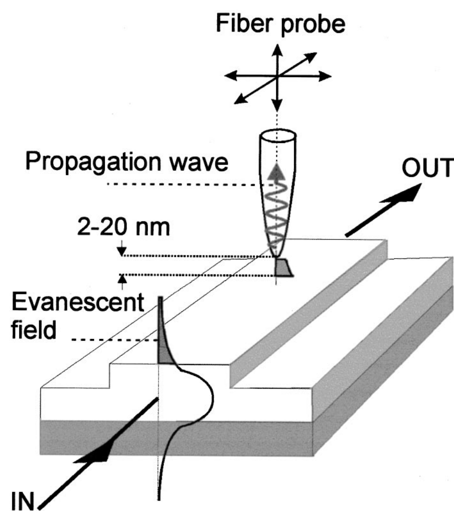

FIG. 1. PSTM is based on the principle of frustration of the evanescent field at the air–waveguide interface when a tapered optical fiber tip is brought in the near field of this interface.

tilevered atomic force microscope (AFM) probes as an alternative to probe the evanescent field and applied the method to image the optical field in a *Y*-junction wavelength (de)multiplexer.[11] Also we looked with a fiber probe based PSTM inside a microcavity.[12] Recently, photonic crystals have received attention in PSTM investigations.[19,20]

Three different types of probes have been used to probe the evanescent field of a waveguide structure: coated and uncoated fiber probes and microfabricated cantilevered AFM probes. The metal coating of a coated fiber probe has been used to screen efficiently against the incoupling of scattered light.[12] Generally an aluminum layer is deposited on the fiber and focused ion beam milling can be used to obtain a highly reproducible subwavelength aperture for the light collection with subwavelength resolution.[22] Of course, an uncoated fiber is easier to fabricate and a higher collection efficiency can be obtained (typically 10^2 more relative to a coated fiber). However, the uncoated probe is very sensitive to scattered light. Also cantilevered AFM probes are sensitive for scattering, when not coated.[11,17] As an advantage, the topography of the waveguide surface can be obtained with these AFM probes, thanks to the possibility of using the cantilever simultaneously as a force sensor using optical beam deflection detection. Due to the critical incoupling of the light into the integrated optical waveguide, it is not possible to scan the waveguide instead of the probe.[17] As a consequence, for the AFM probe, both the optical beam deflection system and the photon tunneling detector have to be scanned together with the probe. Furthermore, the coupling of the photon tunneling signal to the detector for an AFM probe is not so straightforward.[11,17] In the case of a flexible tapered coated or uncoated fiber probe, it is not necessary to scan the photon tunneling detector together with the fiber probe. Thus, uncoated fiber probes are preferred to obtain subwavelength optical PSTM maps of high-quality/low-loss waveguide structures.[12] Instead, for the investigation of strongly scattering waveguide structures, the coated fibers are recommended to diminish the large amount of scattered light.

Different types of height feedback systems for the probe have been used to scan the probe over the waveguide, either on the constant intensity level of the photon tunneling signal[15] or on force interaction.[5,11–14,16–20] In the case of constant intensity feedback, the distance between the fiber probe and the waveguide surface varies. Using the force interaction feedback, this distance is kept constant. A drawback of the constant intensity feedback mode is that the fiber probe and the waveguide can come in contact during the scan.[15] This can be prevented using a height feedback system based on force interaction.[5,11–14,16–20] The force feedback with a cantilevered probe is based on the optical detection of the beam deflection.[11,17] For the fiber probes, there are two possibilities: shear-force feedback using optical detection[14] or using a tuning fork.[12,13,18] A drawback of the shear-force feedback based on optical detection is the interference with the photon tunneling signal, which is prevented with the nonoptical shear-force feedback based on a tuning fork.[12,13,18] As a major advantage all types of height regulation systems based on force interaction yield the topography of the waveguide surface simultaneously with the probing of the optical field in the waveguide.[11,12,13,18]

Conventional piezoelectric tube scanners with a typically scan range of maximum $60\times 60\,\mu\text{m}^2$ have been used to scan the probe over the waveguide surface.[1,15–17,23–25] The width of integrated optical ridge waveguides is, in general, some micrometers over a length of millimeters up to centimeters. The height of such a waveguide varies between some nanometers and micrometers. Thus, the conventional piezoelectric tube scanners do not fulfill all these demands and a larger area scanner is needed for this purpose.

In the design of our PSTM for quantitative microscopy of the field distribution of the light in a waveguide and the waveguide dimensions, we have taken many demands into account. In the following, we present a stand-alone PSTM based on fiber probes combined with a tuning fork shear-force microscope that allows real time and nondestructive imaging of the optical intensity distribution in integrated optical waveguides. A new large area piezoelectric scanner has been constructed and allows to scan an area of a waveguide in the order of centimeters with an accuracy in the height direction of 0.5 nm. With this microscope it is possible to measure quantitatively and simultaneously the optical field and topography of high-quality/low-loss waveguides. The performance of the microscope is illustrated with two examples: a splitter in a Mach–Zehnder interferometer and a mode mixer. A quantitative comparison between the measured optical field distribution in the waveguides and those simulated, using the two-dimensional (2D) finite difference beam propagation method (2D-FD-BPM)[26,27] and a 2D mode solver is made.

II. EXPERIMENTAL

A. Setup for optical intensity imaging

The stand-alone PSTM has been combined with a shear-force microscope using a tuning fork as force sensor. The fiber is attached rigidly to one of the prongs of a 32.8 kHz piezoelectric tuning fork, as shown in Fig. 2.[28] the tuning

Downloaded 01 Sep 2003 to 130.89.25.109. Redistribution subject to AIP license or copyright, see http://ojps.aip.org/japo/japcr.jsp

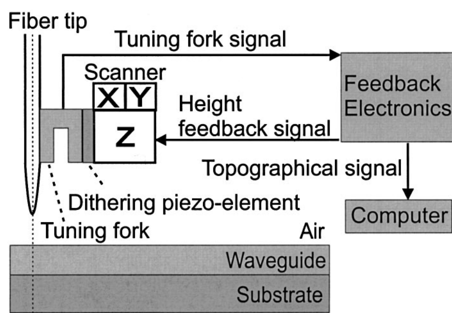

FIG. 2. Shear-force height feedback based on tuning forks is used to obtain a topographical image of the air–waveguide interface.

fork is mechanically dithered at its resonance frequency with a dithering piezoelement. The amplitude or the phase response of the quartz crystalline piezoelectric tuning fork is detected.[29] Approaching the fiber probe to the surface of the waveguide causes the amplitude and phase of the signal to reduce and shift, respectively, due to shear forces acting between surface and probe. The distance dependence of this signal is used in a feedback loop to position the probe at a constant distance of about 10 nm above the waveguide using a piezoelectric scanner. The height feedback signal in this feedback loop contains the height information of the waveguide surface. The height sensitivity of the shear-force detection system is 0.5 nm.

The setup for imaging the optical intensity is shown in Fig. 3. Light from a He–Ne laser with wavelength 632.8 nm is coupled into the waveguide using a microscope objective. To probe the evanescent field we have used uncoated single-mode tapered optical fibers. Light coupled from the evanescent field into the fiber probe is guided trough the fiber to a photomultiplier tube which has an optical sensitivity of 3 fW (dark level) for a wavelength of 632.8 nm. The detected signal is proportional to the intensity of the evanescent field. An incoupled laser power of 5 mW results in a detected photon-tunneling signal in the order of nW's. The detected power is dependent on the fraction of the evanescent power at a certain height relative to the incoupled power into the waveguide and the coupling of the evanescent light into the fiber

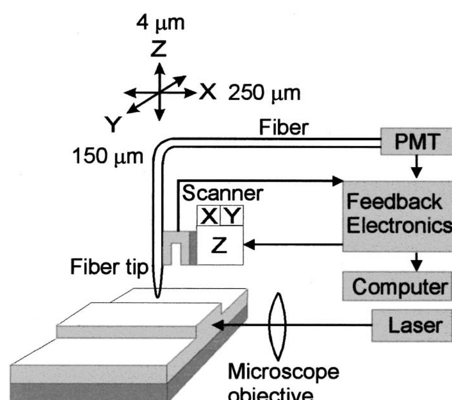

FIG. 3. Setup for imaging the optical intensity distribution in integrated optical waveguides. Light from the laser is coupled into the waveguide. The evanescent field is probed by scanning an optical fiber tip above the surface of the waveguide.

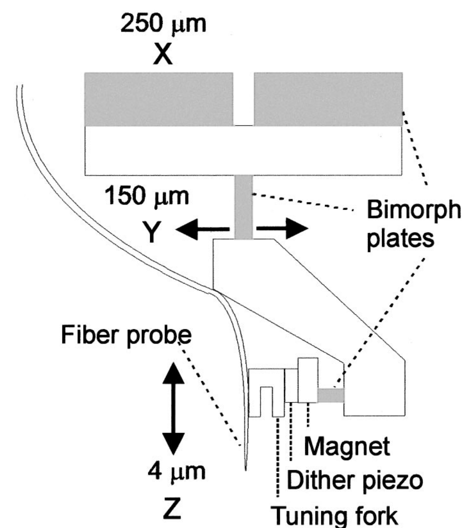

FIG. 4. *XYZ*-piezoelectric bimorph scanner. Perspex has been used to connect the bimorph plates together. These bimorph plates bend when a voltage is applied (−150 to +150 V). The fiber probe is attached to the tuning fork and dither piezoelement and attached to the *z*-bimorph plate with a magnet. The attachment with a magnet allows probe replacement within a couple of minutes. The scanner has a range of 250, 150, and 4 μm in the *x*, *y*, and *z* direction, respectively, applying −150 to 150 V.

probe. The fiber probe is scanned over the waveguide surface while the waveguide is kept fixed in the setup.

For this specific application a new *XYZ*-piezoelectric bimorph scanner has been developed with a large scan range and a high resonance frequency of 350 Hz to obtain large area images of the waveguides combined with fast scanning. This scanner has been constructed using piezoelectric bimorph plates. A schematic side view of the scanner is shown in Fig. 4. The scanner has a range of 250, 150, and 4 μm in the *x,y,z* directions, respectively. With a range of 4 μm in the *z* direction it is possible to measure height steps of some nanometers and to compensate for a possible tilt between the $x-y$ scan plane and the waveguide. The stability of the scanner in the lateral direction is 5 nm. A position feedback system has been built in to compensate for the nonlinearity of the piezoelectric bimorph scanner, resulting in a deviation from linearity of less than 2%. The scanner is mounted to a tripod system for the coarse approach of the fiber probe to the waveguide structure. The *z*-piezo element is used for the fine approach. The whole scanner can be translated with μm-translation stages in the *x* and *y* direction over 50 mm to position the scan area at the device position of interest.

With this combined photon tunneling and tuning fork shear-force microscope, it is possible to measure directly and simultaneously the optical field distribution of the light in high-quality/low-loss waveguides and the dimensions of the waveguides with only one probe. The method is nondestructive and *in situ* with a subwavelength resolution. The waveguides can be imaged over 50 mm in the lateral direction with a height sensitivity of 0.5 nm.

B. Waveguides

We have performed quantitative PSTM on two different ridge waveguides. First, a Si_3N_4 Mach–Zehnder

Downloaded 01 Sep 2003 to 130.89.25.109. Redistribution subject to AIP license or copyright, see http://ojps.aip.org/japo/japcr.jsp

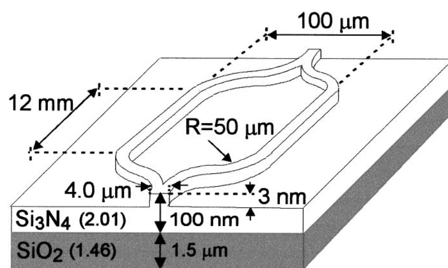

FIG. 5. Design of the integrated Mach–Zehnder interferometer with a working wavelength of 632.8 nm. A 1.5 μm SiO_2 layer with a refractive index of 1.46 is used as the cladding layer. On this SiO_2 layer, a high-index Si_3N_4 waveguide layer with a refractive index of 2.0 and a thickness of about 100 nm is deposited by chemical vapor deposition. The guiding layer consists of a ridge structure with a height of 3 nm and a width of 4.0 μm. The waveguide channels are monomodal in the direction normal to the waveguide surface and bimodal in the plane of the waveguide surface. The evanescent field outside the waveguide contains about 12% of the light power coupled into the modes and the decay length of the intensity of the evanescent field of the TE_{00} and TE_{01} mode is 41 (2) nm. The incoupling efficiency of the HeNe-laser light via a microscope objective in the incouple waveguide of the interferometer is about 2%.

interferometer.[30] The interferometer is part of an immunosensor[30] for the direct detection of antigen binding to antibody receptor molecules immobilized on the waveguide surface. Second, a SiON mode-splitting junction.[2] Multibranch junctions,[2] which can spatially separate the modes of a channel waveguide are used for a multitude of functions such as selective mode excitation, mode routing, and multiport broad-band wavelength multiplexing and demultiplexing.

1. Mach–Zehnder interferometer

The Mach–Zehnder sensor uses the evanescent field to detect small refractive-index changes near the guiding-layer surface.[30] The highest sensitivity can be attained with symmetrical mono-mode channels. In the Mach–Zehnder interferometer the light enters a first *Y* junction where it is split into a sensing branch and a reference branch and recombined in a second *Y* junction. When after the first *Y* junction the sensing branch interacts with a sample to be analyzed, a phase shift ϕ between both branches will occur. The light intensity, in this case, is related to the phase shift ϕ. The design of the Mach–Zehnder interferometer with a working wavelength of 632.8 nm is shown in Fig. 5. For the measurement, a linearly polarized HeNe laser beam with a laser power of 5 mW and a wavelength of 632.8 nm has been coupled into the interferometer with a 40×, $NA=0.65$ microscope objective. In the following a mode is presented as TE_{kn} with k and n the mode numbers in the directions normal and parallel to the waveguide, respectively.

2. Mode-splitting Y junction

Multibranch junctions can spatially separate the modes of a channel waveguide.[2] Two distinct effects, i.e., mode localization and adiabatic propagation cause the mode-splitting behavior of multibranch junctions.[2] Therefore, power launched in one of the modes of the multi-modal branch will end up in only one of the branches of the junction. Essentially, the device is reversible, e.g., power launched in one of the branches will end up in one particular mode of the multi-modal branch. The localization of the modal profile for the TM_{02} mode of a mode-splitting *Y* junctions is illustrated in Fig. 6.

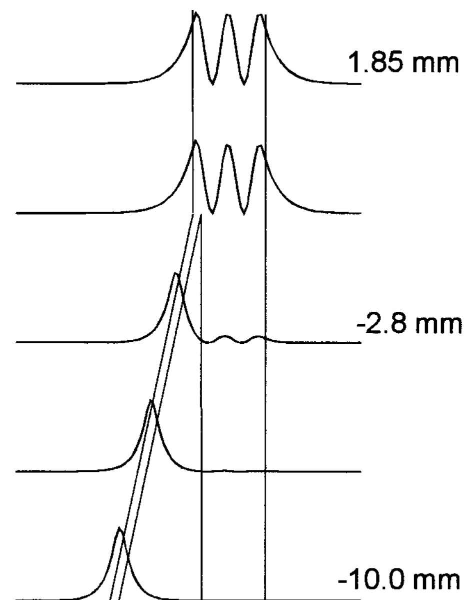

FIG. 6. Localization of the modal profile for the TM_{02}-system mode of a mode-splitting *Y* junction (top view) for increasing separation between the branches.

The mode-splitting *Y* junction, which is schematically shown in Fig. 7, has been designed for the investigation of a mode-splitting Ψ junction.[2] When the light is coupled in the 2 μm branch of the junction a TM_{02}-mode will be generated in the multi-modal branch. Crosstalk will result in a beat pattern between the modes in the multi-modal branch. So, a measurement of the optical intensity distribution with the PSTM will not only show the performance of the device, but will also give a good indication of the amount of crosstalk between the different modes. For the investigated mode-splitting *Y* junction, we expect crosstalk mainly between TM_{01} and TM_{02} with a beat length of about 1.8 mm. For the

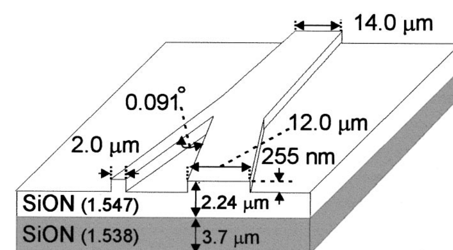

FIG. 7. Design of the mode-splitting *Y* junction. The guiding layer made in SiON consists of a ridge structure with a height of 255(13) nm and a width of 2, 12, and 14 μm for the different branches, respectively (see Ref. 2). The guiding and the buffer layer have a thickness of 2.24(2) μm, 3.70(4) μm, respectively. For the refractive indices of the guiding and the buffer layer, is 1.538(2), and 1.547(2), respectively. The lateral refractive index contrast is $8.5(2)\times10^{-4}$ and the angle between the two branches is about 0.091°. The evanescent field outside the waveguide contains about 5% of the light power coupled into the modes and the decay length of the TM_{02} mode is about 360 nm.

Downloaded 01 Sep 2003 to 130.89.25.109. Redistribution subject to AIP license or copyright, see http://ojps.aip.org/japo/japcr.jsp

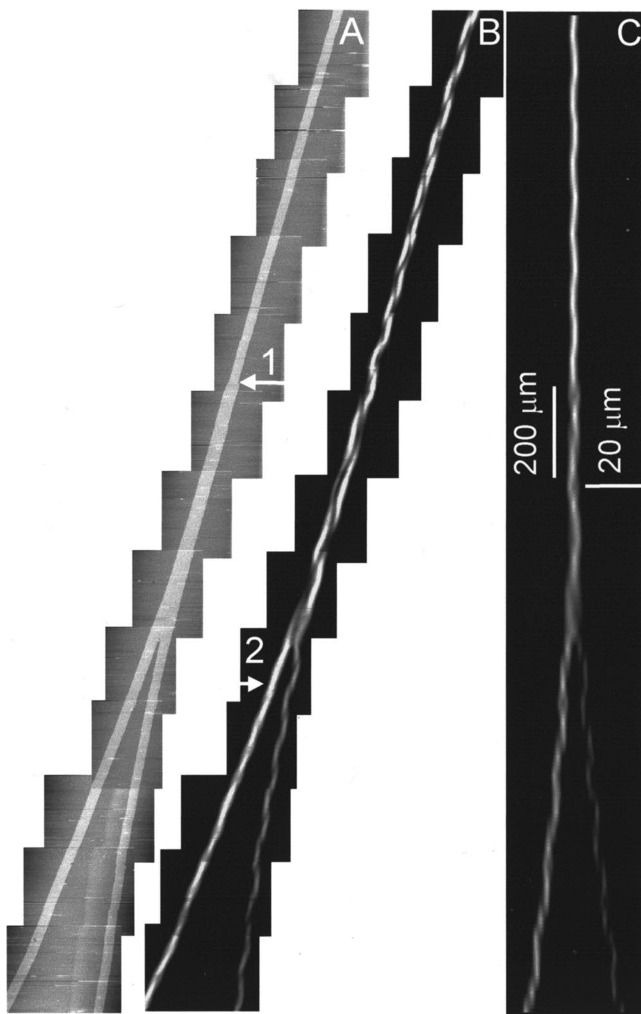

FIG. 8. PSTM measurement and a BPM simulation of the Mach–Zehnder interferometer at the first *Y* junction. (a) The measured topography. The height of the step is 4.1(5) nm. (b) The simultaneously measured optical intensity distribution. The light propagates from the top to the bottom of the image. (c) The simulated optical intensity distribution with a 2D-FD-BPM (see Refs. 26 and 27).

measurement, a linearly polarized HeNe laser beam with a laser power of 10 mW and a wavelength of 632.8 nm has been coupled into the 2 μm branch of the mode splitter with a 40×, $NA=0.40$ microscope objective.

III. RESULTS

A. Mach–Zehnder interferometer

The optical intensity distribution at the first *Y* junction of the interferometer has been imaged simultaneously with its topography. The topography is shown in Fig. 8(a) together with the optical intensity distribution in Fig. 8(b). After each scan, the scanner was translated over 170(3) μm in the propagation direction of the light to obtain a new scan. This way, an image at the first *Y* junction over a total length of 2.20(4) mm has been obtained by concatenating 13 scans. For the first ten scans, a scan area of 25.0(5) μm by 200(4) μm has been used and for the last three, a scan area of 40.0(8) μm by 200(4) μm. Each image consists of 200 $\times$200 pixels with a pixel size of 1.00(2) μm in the propagation direction. The pixel size perpendicular to the propagation direction for the 25μm$\times$200μm and the 40μm $\times$200μm scans were 125(3) nm and 200(4) nm, respectively. The measuring time per image was about seven minutes with a line scan frequency of 0.5 Hz and a pixel frequency of 100 Hz.

The topographical map of the first *Y* junction of the interferometer [Fig. 8(a)] shows a measured height of the ridge of the channel waveguide of about 4 nm. A local defect before the *Y* junction can be observed (arrow 1). The width of the channel waveguide before entering the *Y* junction at the position of the local defect becomes abruptly larger due to the multiple exposure of the mask. The optical image of Fig. 8(b) shows the intensity of the optical field, which propagates from the top to the bottom of the image. A mode-beat pattern, corresponding to a bimodal behavior of the interferometer is observed before the *Y* junction. The mode-beat length increases with the width of the channel waveguide. After the *Y* junction, the light is split into the two branches of the interferometer and the mode beats are still observed in both branches. The mode-beat length in the two branches is slightly different, due to the difference in the width of the two channel waveguides, which in turn leads to a different wavelength difference between the excited modes. In Fig. 8(c), the simulation of the intensity distribution is presented, which has been obtained, using the 2D-FD-BPM.[26,27] A Gaussian beam with TE polarization, a width of 2.5 μm, and a launching angle of 1.0° into the waveguide has been used for the simulation. The simulation indicated that the mode-beat pattern is due to the interference of the TE_{00} mode with the TE_{01} mode. The period of simulated mode-beat pattern [Fig. 8(c)] corresponds well with the period of the measured mode-beat pattern [Fig. 8(b)]. However, there is a slight difference between the measured and the simulated shape of the mode-beat patterns.

Line plots of the measured height and the optical signal at 100 μm after the first *Y* junction in Fig. 8(a) (arrow 2) are shown in Fig. 9. The height of the ridge at this place is 4.1(5) nm and the measured optical power is 2.5(5) nW. The line plot of the height illustrates that the Mach–Zehnder interferometer is not symmetrical. The width of one branch is 4.1(2) μm and of the other, 3.6(2) μm. This asymmetry decreases the maximally obtainable visibility of fringes in the interferometer.

B. Mode-splitting junction

The optical intensity distribution of the mode-splitting junction at the splitting point has also been measured simultaneously with its topography. The topography is shown in Fig. 10(a) and the optical intensity distribution is shown in Fig. 10(b). After each scan, the scanner was translated over 170(3) μm in the propagation direction of the light to obtain a new scan. An image at the splitting point over a total length of 1.87(4) mm has been obtained by attaching 11 scans together. Another scan at 2.80(6) mm before the splitting-point has been used to determine the angle between the two smallest branches. This angle is 0.092°(2) and is in good correspondence with the design angle of 0.091°. A scan area of

Downloaded 01 Sep 2003 to 130.89.25.109. Redistribution subject to AIP license or copyright, see http://ojps.aip.org/japo/japcr.jsp

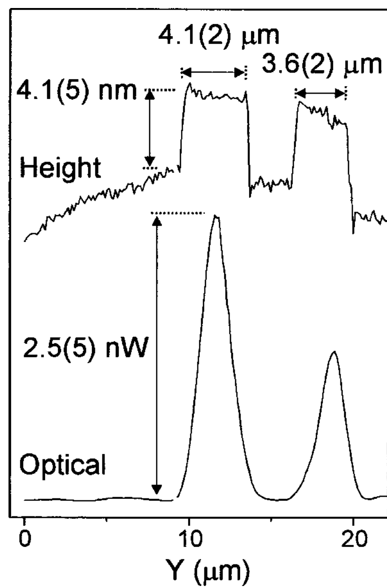

FIG. 9. Line plots of the measured (a) height and (b) optical signal at 100 μm after the first *Y* junction [see arrow 2 in Fig. 8(b)].

60(1) μm by 200(4) μm has been used. Each image consists of 200 pixels by 200 pixels with a pixel size of 1.00(2) μm times 300(6) nm (*x* direction is perpendicular to the propagation direction of the light). The measuring time per image was about seven minutes with a line scan frequency of 0.5 Hz and a pixel frequency of 100 Hz.

The optical image [Fig. 10(b)] shows how the light propagates in the mode-splitting junction from the bottom to the top of the image. At 2.8 mm before the junction, almost all the light is coupled in the 2 μm branch and a small part in the 12 μm branch. After the junction, a TM_{02} mode is generated in the 14 μm multi-modal branch. Beside the three peaks of the TM_{02} mode in the multi-modal branch also two ''peaks'' of the lateral evanescent field outside the waveguide can be observed in Fig. 10(b). The expected mode-beat length of about 1.8 mm between the TM_{01} and TM_{02} mode is not observed. The 2D-FD-BPM[26,27] simulation of the generation of the TM_{02} mode in the multi-modal branch over a length of 1.87(4) mm is shown in Fig. 10(c), where the power has been launched into the 2 μm branch.

Line plots of the measurements and the simulation can be seen in Figs. 11 and 12 at the location of arrows 1 and 2 in Fig. 10, respectively. The line plots of the measured height [Fig. 11(a)/12(a)] and optical signal [Fig. 11(b)/12(b)] are shown. Also, the line plots of the simulations [Fig. 11(c)/12(c)] with the 2D-FD-BPM[26,27] method are shown. The measured optical field of Fig. 11(b) shows besides the three maxima of the TM_{02} mode also two peaks of the evanescent field outside the waveguide. These peaks are caused by the height difference of 250(20) nm between the top of the waveguide and next to the waveguide. The height of the ridge, when compared to a position close to but next to the ridge, results in an increase in distance from the point of highest intensity of the mode. As a result, the optical field detected on top of the ridge is reduced with respect to a position next to the ridge. These peaks can not be observed in the line plot of the 2D-FD-BPM simulation of Fig. 11(c).

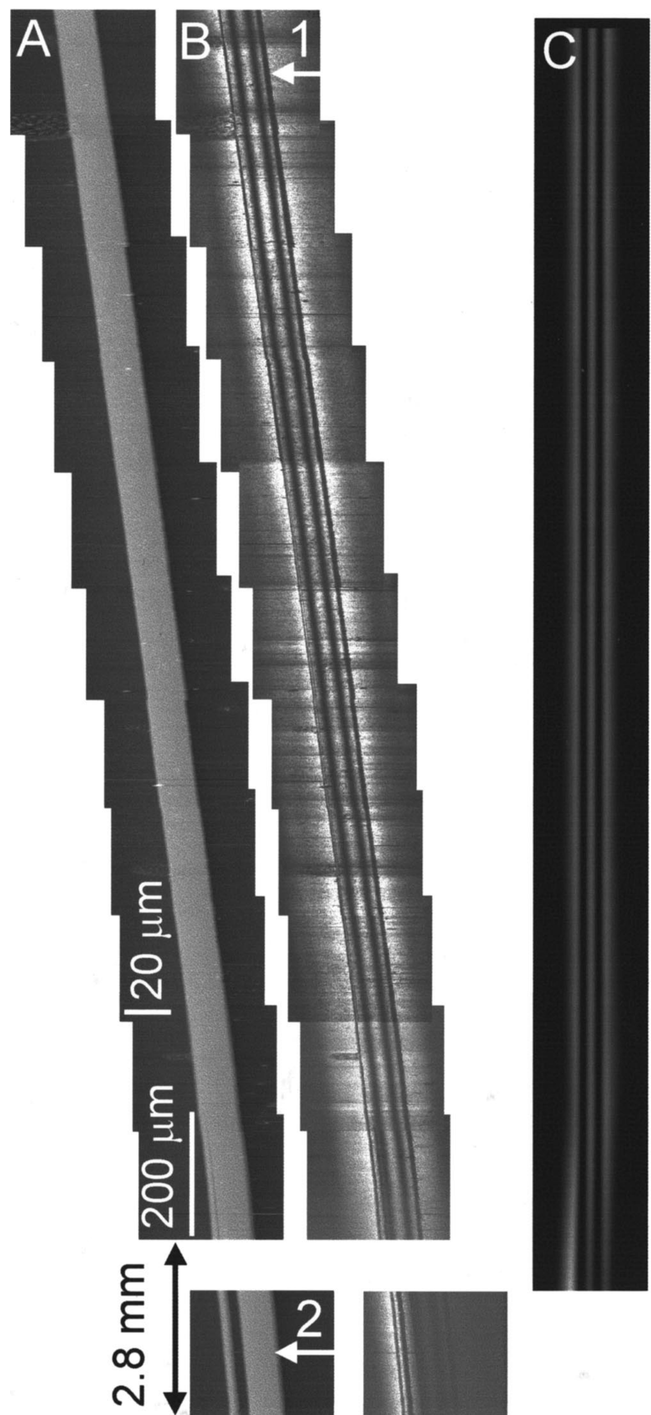

FIG. 10. PSTM measurement and a BPM simulation of the mode-splitting junction. (a) The measured topography. The height of the step is about 250(20) nm. (b) The simultaneously measured optical intensity distribution. The light propagates from the bottom to the top of the image. (c) The simulated optical intensity distribution with a 2D-FD-BPM (see Refs. 26 and 27).

To include the height difference in the measurement of 250 nm in the simulation a 2D mode solver has been used. The results of this simulation are shown in Fig. 11(d). They indicate that the two peaks of the evanescent field outside the waveguide are indeed due to the 250 nm height step in the measurement. The line plot of the 2D-FD-BPM simulation of Fig. 12(c) shows one peak in the small branch and two little

Downloaded 01 Sep 2003 to 130.89.25.109. Redistribution subject to AIP license or copyright, see http://ojps.aip.org/japo/japcr.jsp

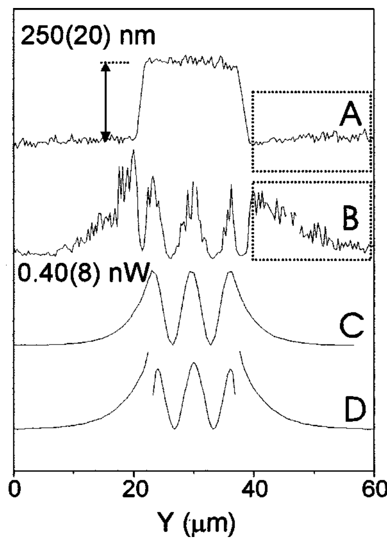

FIG. 11. Line plots of the PSTM measurements and simulations at the place of arrow 1 of Fig. 10. (a) The measured height and (b) optical signal. The simulations with the (c) 2D-FD-BPM (see Refs. 26 and 27) and the (d) 2D mode solver. The measured height of the step and the measured optical power is 250(20) nm and 0.40(8) nW, respectively.

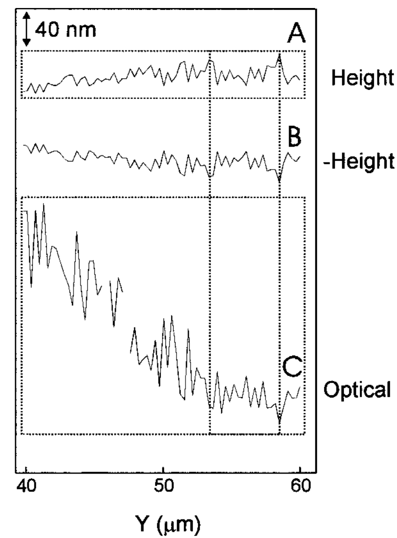

FIG. 13. Influence of the surface roughness of the mode-splitting junction on the measured optical intensity. (a) Zoom out of a part of the line plot of the measured height of Fig. 11(a). (b) The inversion of (a). (c) Zoom out of a part of the line plot of the measured optical signal of Fig. 11(b).

peaks in the wider branch. The measured optical field at this position [Fig. 12(b)] shows also these three peaks with the same peak-to-peak ratio. The two extra observed peaks of the evanescent field outside the small branch [Fig. 12(b)] are also due to the 250 nm height step in the measurement.

The surface roughness of the junction has influence on the measured optical intensity. To illustrate this, part of the line plots of the measured height [Fig. 11(a)] and the optical signal [Fig. 11(b)] are magnified in Fig. 13(a) and Fig. 13(c), respectively. When the line plot of the inverted height signal [Fig. 13(b)] is compared with the line plot of the optical signal [Fig. 13(c)] a clear correlation is observed between the peaks and the dips in the height and the optical measurement.

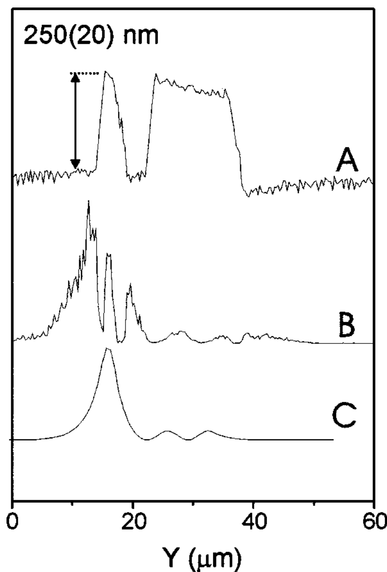

FIG. 12. Line plots of the PSTM measurements and simulations at the place of arrow 2 of Fig. 10. (a) The measured height and (b) optical signal. The simulations with the (c) 2D-FD-BPM (see Refs. 26 and 27).

At the point where the height signal increases, due to the surface roughness, a decrease of the optical signal is observed. This is also a result of an increase in distance from the point of highest intensity of the mode. The surface roughness of the waveguide has also been measured with an AFM. With both the AFM and the PSTM, we find a roughness of 5 nm root-mean-square. The 2D mode solver has been used to simulate the optical intensity at a height of 5, 10, and 15 nm, respectively above the waveguide surface. These calculations confirm that the variations in the measured optical signal are caused by the variations in the height signal, due to the surface roughness.

IV. DISCUSSION

A. Mach–Zehnder interferometer

The comparison of the measured and calculated optical intensity distribution in the Mach–Zehnder interferometer shows good agreement in the general behavior and yields more detailed information about the fabrication and the performance of the interferometer. Firstly, the interferometer is bimodal and the device is not totally symmetric. These imperfections will have a negative influence on the sensitivity of the device. The fabrication of the device should be improved to obtain a more symmetric structure and a monomodal behavior. Secondly, the fabricated guiding layer has a slightly different thickness than the expected thickness of 100 nm or the SiO2 layer has a different refractive index than the expected index of 1.46. This can be concluded from the fact that the measured mode beat length between the TE_{00} mode and the TE_{01} mode in the channel waveguide before the *Y* junction is a factor 1.2 larger than the simulated mode beat length. Thirdly, we found that the PSTM measurements are sensitive for the launching angle by analyzing the measured mode-beat pattern. Thus, effects due to the launching angle can be explained. Fourth, a small shift of the laser beam out of the center of the waveguide or a small

Downloaded 01 Sep 2003 to 130.89.25.109. Redistribution subject to AIP license or copyright, see http://ojps.aip.org/japo/japcr.jsp

angle of the laser beam gives a different optical intensity distribution. This means that the coupling of the laser beam into the interferometer is very critical. All this information and the observed defect in the topography [indicated with arrow 1 in Fig. 8(a)] constitute valuable information for better design, fabrication, and understanding of the operation of the interferometer.

B. Mode-splitting junction

The measured mode profile in the multi-modal branch corresponds well with the calculated mode profile of a TM_{02} mode. The observation of the TM_{02} mode and the absence of mode beating in Fig. 10(b) indicate that the mode splitter works properly as designed. With these PSTM measurements we have been able to check the performance of the mode splitter and to determine the surface roughness of the mode splitter.

The surface roughness and the 250 nm height step of the waveguide introduce artifacts in the measured optical intensity. In principle, it should be possible to correct the measured intensity distribution using the measured topography of the waveguide. This is an advantage of the simultaneous measurement of the optical field and the topography. A more elegant method to measure without surface artifacts would be to measure at a constant height above the wafer surface, instead of measuring with a constant distance between the probe and the wafer surface.

V. CONCLUSIONS

Quantitative maps of the optical field distribution in high-quality/low-loss integrated optical waveguides have been obtained with a stand-alone PSTM based on fiber probes combined with a tuning fork shear-force microscope. Simultaneously, the topography of the waveguides is recorded with subnanometer accuracy. This method measures the field patterns locally, directly, *in situ*, and is nondestructive for the waveguide. The new developed piezoelectric bimorph scanner is capable to map large waveguides with lengths up to 50 mm and has a height sensitivity of 0.5 nm. The performance of the PSTM is verified by investigating a planar waveguide splitter and mixer with the microscope. Although good qualitative agreement between experimental and simulated field patterns is obtained the experiment also reveals detailed deviations due to incoupling conditions, mask imperfections, waveguide edges, and surface roughness. We showed that the PSTM can be used to optimize the design of integrated optical waveguides, to verify their performance, and for a better understanding of the operation of integrated optical structures.

ACKNOWLEDGMENTS

This work is part of the strategic research orientation on ''advanced photonic structures'' of the MESA$^+$ Research Institute. Furthermore, this work is part of the research program of the ''Stichting voor Fundamenteel Onderzoek de Materie (FOM),'' which is financially supported by the ''Nederlandse Organisatie voor wetenschappelijk Onderzoek (NWO).'' The authors want to thank BBV-Software BV for the 2D mode solver program and Selene and Eddy Schipper for the Mach–Zehnder interferometer.

[1] S. I. Hosain, J. P. Meunier, E. Bourillot, F. De Fornel, and J. P. Goudonnet, Fiber Integr. Opt. **14**, 89 (1995).
[2] G. J. Veldhuis, J. H. Berends, and P. V. Lambeck, J. Lightwave Technol. **14**, 1746 (1996).
[3] C. van Dam, J. W. M. van Uffelen, M. K. Smit, G. N. van den Hoven, A. Polman, L. Shi, L. H. Spiekman, X. J. M. Leijtens, Proceedings of the Seventh European Conference on International Optics, **1**, Delft, Netherlands, 3-6 April, 25 (1995).
[4] E. Betzig and J. K. Trautman, Science **257**, 2484 (1992).
[5] M. Svalgaard, S. Madsen, J. M. Hvam, and M. Kristensen, IEEE Photonics Technol. Lett. **10**, 848 (1998).
[6] D. Courjon, K. Sarayeddine, and M. Spajer, Opt. Commun. **71**, 23 (1989).
[7] F. de Fornel, J. P. Goudonnet, L. Salomon, and E. Lesniewska, Proc. SPIE **1139**, 77 (1989).
[8] R. C. Reddick, R. J. Warmack, D. W. Chicott, S. L. Sharp, and T. L. Rerrel, Rev. Sci. Instrum. **61**, 3669 (1990).
[9] N. F. van Hulst, N. P. de Boer, and B. Bölger, J. Microsc. **163**, 117 (1991).
[10] S. Jiang, N. Tomita, H. Ohsawa, and M. Othsu, Jpn. J. Appl. Phys., Part 1 **30**, 2107 (1991).
[11] E. G. Borgonjen, M. H. P. Moers, A. G. T. Ruiter, and N. F. van Hulst, Proc. SPIE **2535**, 125 (1995).
[12] M. L. M. Balistreri, D. J. W. Klunder, J. P. Korterik, F. C. Blom, A. Driessen, H. W. J. M. Hoekstra, L. Kuipers, and N. F. van Hulst, Opt. Lett. **24**, 1829 (1999).
[13] M. L. M. Balistreri, J. P. Korterik, A. Driessen, L. Kuipers, and N. F. van Hulst, Opt. Lett. **25**, 637 (2000).
[14] D. P. Tsai, H. E. Jackson, R. C. Reddick, S. H. Sharp, and R. J. Warmack, Appl. Phys. Lett. **56**, 1515 (1990).
[15] E. Bourillot, F. De Fornel, J. P. Goudonnet, D. Persegol, A. Kevorkian, and D. Delacourt, J. Opt. Soc. Am. A **12**, 95 (1995).
[16] Y. Toda and M. Ohtsu, IEEE Photonics Technol. Lett. **7**, 84 (1995).
[17] A. Mannoni, F. Quercioli, B. Tiribilli, C. Ascoli, P. Baschieri, and C. Frediani, J. Lightwave Technol. **16**, 388 (1998).
[18] G. H. Van der Rhodes, B. B. Goldberg, M. S. Ünlü, S. T. Chu, W. Pan, T. Kaneko, Y. Kokobun, and B. E. Little, Appl. Phys. Lett. **75**, 2368 (1999).
[19] E. B. MacDaniel, J. W. P. Hsu, L. S. Goldner, and R. J. Tonucci, Phys. Rev. B **55**, 10878 (1997).
[20] P. L. Phillips, J. C. Knight, B. J. Mangan, P. St. J. Russell, M. D. B. Charlton, and G. J. Parker, J. Appl. Phys. **85**, 6337 (1999).
[21] A. G. Choo, H. E. Jackson, U. Thiel, G. N. De Brabander, and J. T. Boyd, Appl. Phys. Lett. **65**, 947 (1994).
[22] J. A. Veerman, A. M. Otter, L. Kuipers, and N. F. van Hulst, Appl. Phys. Lett. **72**, 3115 (1998).
[23] A. J. Meixner, M. A. Bopp, and G. Tarrach, Appl. Opt. **33**, 7995 (1994).
[24] D. Courjon, C. Bainier, and F. Baida, Opt. Commun. **110**, 7 (1994).
[25] A. G. Choo, M. H. Chudgar, H. E. Jackson, G. N. De Brabander, M. Kumar, and J. T. Boyd, Ultramicroscopy **57**, 124 (1995).
[26] H. J. W. M. Hoekstra, G. J. M. Krijnen, and P. V. Lambeck, J. Lightwave Technol. **10**, 1352 (1992).
[27] H. J. W. M. Hoekstra, H. J. van Weerden, P. V. Lambeck, and Th. J. A. Popma, IEEE Photonics Technol. Lett. **6**, 83 (1994).
[28] K. Karrai and R. D. Grober, Appl. Phys. Lett. **66**, 1842 (1995).
[29] A. G. T. Ruiter, J. A. Veerman, K. O. van der Werf, and N. F. van Hulst, Appl. Phys. Lett. **71**, 28 (1997).
[30] E. F. Schipper, A. M. Brugman, C. Dominguez, L. M. Lechuga, R. P. H. Kooyman, and J. Greve, Sens. Actuators B **40**, 147 (1997).

Downloaded 01 Sep 2003 to 130.89.25.109. Redistribution subject to AIP license or copyright, see http://ojps.aip.org/japo/japcr.jsp